Nisbet, H., Migdisov, A. A., Goncharov, V., van Hinsberg, V., Williams-Jones, A., Xu, H., and Guo, X., 2022,
The solubility and speciation of Nd in carbonate-bearing hydrothermal fluids up to 250° C: Chemical Geology, v. 611, p. 121122.

The solubility and speciation of Nd in carbonate-bearing hydrothermal fluids up to 250°C

Haylea Nisbet[1,2], Artas Migdisov[1], Vitaliy Goncharov[3], Vincent van Hinsberg[2], Anthony Williams-Jones[2], Hongwu Xu[1], Xiaofeng Guo[3]

[1]Earth and Environmental Sciences Division, Los Alamos National Laboratory, Los Alamos, New Mexico, 87545, USA.

[2]GEOTOP research centre, Department of Earth and Planetary Sciences, McGill University, 3450 University Street, Montreal, Quebec, H3A 0E8, Canada.

[3]Alexandra Navrotsky Institute for Experimental Thermodynamics, Washington State University, Pullman, Washington 99164, United States

1. Abstract

Neodymium is one of the most sought-after Rare Earth Elements (REE), owing to its use in permanent magnets. In nature, the enrichment of Nd and other REE is frequently attributed to their transport and deposition by hydrothermal fluids. Whereas numerous studies have investigated the complexation of Nd with chloride, sulfate, and fluoride in hydrothermal fluids, a major gap in understanding that hinders our ability to predict the mobility of Nd in ore-forming hydrothermal systems is its behavior in carbonate-bearing fluids at elevated temperature. In this contribution, we determine the speciation of Nd in carbonate-bearing fluids under acidic (pH_T 2 − 4) and alkaline (pH_T 7.8 − 9.8) conditions by the autoclave solubility method at temperatures between 175 and 250°C using synthesized Nd-hydroxylbastnäsite as the reference phase. We demonstrate that the predominant aqueous complexes are $NdCO_3^+{}_{(aq)}$ and $NdCO_3OH^0{}_{(aq)}$ under acidic and alkaline conditions, respectively. Our findings predict that carbonate species predominate over chloride species at alkaline pH and that carbonate thus has the potential to be an important ligand for REE mobilization in hydrothermal fluids.

2. Introduction

The Rare Earth Elements (REE) have become an essential resource in the 21st-century due to their indispensable use in advanced technologies, particularly in green energy initiatives (wind turbines, electric cars), the production of permanent magnets, and national security strategies (satellites, aircraft) (Van Gosen et al., 2017). As a result, the global demand for these elements has increased considerably, and with that, the need to discover and exploit new resources. Contrary to what their name suggests, the REE are relatively plentiful in nature and comparable in crustal abundance to other metals such as Mo, Ni, and Co (Voncken, 2016). Rather, it is their tendency to become concentrated into economic quantities sufficient to achieve "ore" status, that is rare.

Although there are cases where REE ore deposits are proposed to have formed by minerals directly precipitated from a magmatic source (e.g. the Sulphide Queen ore body at Mountain Pass, California; Castor, 2008), growing evidence suggests that, more commonly, hydrothermal fluids mobilize the REE from their source and ultimately concentrate them to ore grades (Migdisov et al., 2016). An important class of REE ore deposits are intimately associated with carbonates: They are hosted in carbonatites (e.g. Bayan Obo, Mountain Pass) and/or contain REE-carbonate minerals such as bastnäsite ($REECO_3(F,OH)$) as the dominant REE ore mineral (Verplanck and Hitzman, 2016). This close association suggests that carbonate-bearing solutions may play a key role in transporting the REE. Indeed, carbonate complexes are among the strongest REE-complexes at ambient conditions (Cantrell and Byrne, 1986; Johannesson and Stetzenbach, 1995), and it has been proposed that this may also hold true at elevated temperatures (Anenburg et al., 2020). In seawater, Cantrell and Byrne (1987) determined that $REECO_3^+$ and $REE(CO_3)_2^-$ are the predominant aqueous complexes, and that the LREE preferentially partition into $REECO_3^+$, and the HREE into $REE(CO_3)_2^-$. Modeling of groundwater from the Nevada Test Site and Yucca

Mountain predicted that the same carbonate complexes for Nd would predominate significantly over Nd-fluoride, chloride, sulfate, and phosphate complexes (Johannesson and Stetzenbach, 1995). A more recent experimental study using potentiometric measurements by Luo and Byrne (2004) corroborated the findings of these studies, and derived thermodynamic formation constants for these species. Data at elevated temperature is limited to theoretical predictions by Wood (1990) and Haas et al. (1995). Unfortunately, these two extrapolations return very different temperature dependencies on the stability of REE-carbonate complexes. Moreover, previous experiments with actinides (Th, U), which share geochemical behaviour aspects with the REE, have demonstrated that temperature can strongly affect the stability of carbonate aqueous complexes when elevated to hydrothermal conditions (Nisbet et al., 2021; Kalintsev et al., 2021). Therefore, reliable data on REE-carbonate speciation at elevated temperatures is required to evaluate the potential for, and importance of REE-carbonate transport in hydrothermal systems.

Of the REE, neodymium (Nd) is among the most highly sought after, owing to its use in permanent magnets: neodymium-iron-boron magnets are currently the strongest magnets in the commercial market (Van Gosen et al., 2017), and are used in technological applications including electronics and green energy. Neodymium is primarily sourced from the REE-carbonate mineral bastnäsite ($REECO_3(F,OH)$), which, in addition to Nd, preferentially hosts Light Rare Earth Elements (LREE) including Ce, La, and Pr, as well as Y, a Heavy Rare Earth Element (HREE) (Voncken, 2016). To date, standard thermodynamic properties of bastnäsite are limited. Shivaramaiah et al. (2016) have reported standard enthalpy of formation values for synthesized Nd-hydroxylbastnäsite by high-temperature oxide melt solution calorimetry, while Gysi and Williams-Jones (2015) used Differential Scanning Calorimetry (DSC) to calculate isobaric heat capacity, and thermogravimetric analysis to derive standard enthalpies of formation and estimate

entropy values, albeit, for a natural bastnasite-(Ce) sample. Our understanding of Nd aqueous complexation at elevated temperatures is restricted to a few studies that investigated the speciation of Nd with ligands that are common in natural hydrothermal systems (Cl^-, F^-, and SO_4^{2-}) (Migdisov and Williams-Jones, 2002; Migdisov et al., 2006; Migdissov and Williams-Jones, 2007). The speciation of Nd in carbonate-bearing solutions at hydrothermal conditions has not yet been investigated experimentally.

In this contribution, we conduct solubility experiments in acidic and alkaline solutions to investigate the aqueous speciation of Nd in carbonate-bearing solutions at conditions relevant to hydrothermal systems.

3. Methods

Solubility experiments were performed in solutions of varying carbonate concentration (0.05-0.5m $NaHCO_3$/Na_2CO_3) and pH to investigate the speciation of Nd in carbonate-bearing hydrothermal fluids at acidic to alkaline pH. Each series of experiments were carried out at 175, 200, 225, and 250°C, and the pressure of saturated water vapor. The experiments used the autoclave solubility technique, described below.

The reference phase used in the experiments was synthesized Nd-hydroxylbastnäsite ($NdCO_3OH$). Bastnäsite, the REE-fluorocarbonate mineral $REECO_3(OH,F)$, is one of the most stable and abundant REE minerals found in REE hydrothermal systems (Shivaramaiah et al., 2016). Whereas, in nature, bastnäsite always occurs as a solid solution that contains multiple LREE and fluorine, we have elected to use end-member Nd-hydroxylbastnäsite in our experiments to simplify the system. The Nd-hydroxylbastnäsite phase was synthesized hydrothermally using the method of Vallina et al. (2014) and Voigt et al. (2016). First, a 50 mM solution of $NdCl_3$ was

mixed with a 50 mM Na_2CO_3 solution at equal proportions to immediately precipitate an amorphous REE carbonate phase. The resulting slurry was added to Teflon-lined titanium autoclaves capped with a Teflon O-ring and heated in a Muffle Furnace that was set at 165-200°C (Vallina et al., 2014; Voigt et al., 2016). The autoclaves were gently shaken every 10 min for the first 60-100 min of heating. After heating for ~3 weeks, the autoclaves were removed from the furnace and cooled to room temperature by a stream of cold air (<30 min). Next, the products were filtered through a glass vacuum filter set-up using 2.5μm filter paper and rinsed several times with deionized water (DI) and isopropyl. The resultant powders were dried at room temperature overnight and analyzed by X-ray Diffraction (XRD) to verify that the correct phase had formed and that the low-temperature polymorph of hydroxylbastnäsite, kozoïte, was not present. To do this, samples were ground into a fine powder, loaded onto a quartz-glass slide, and analyzed by a Bruker D8 Discover X-ray Diffractometer with CuKα radiation ($\lambda = 0.154$ nm, 40 kV, and 40 mA) and a LynxEye position-sensitive detector. Scans were completed from 5 to 70º 2θ with a step size of 0.02º and a dwell time of 1-2 sec per step. The collected patterns (Fig. 1) matched that of Nd-hydroxylbastnäsite obtained by Vallina et al. (2015). The phase was also analyzed by XRD after completion of the experiment to verify that no phase change had occurred.

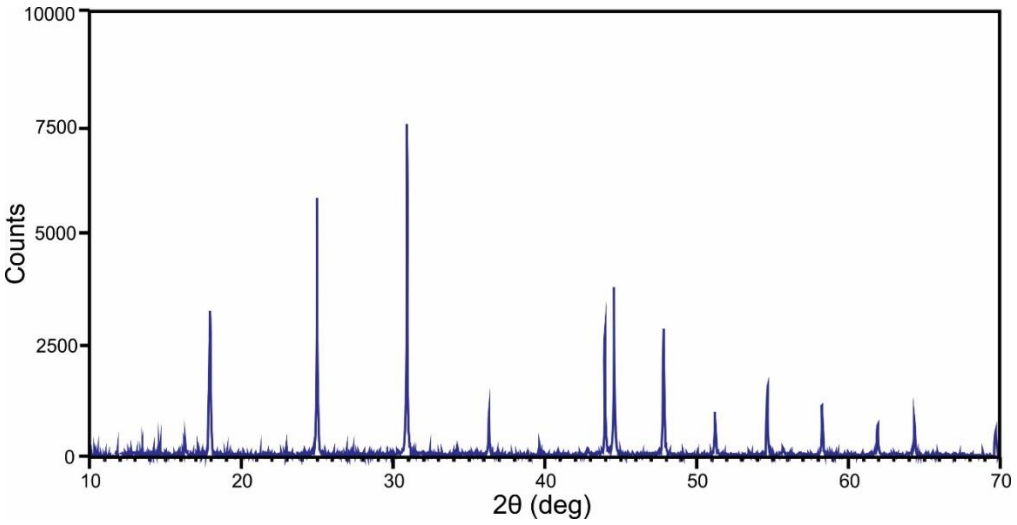

Figure 1. An example of an XRD scan of the reference phase after hydrothermal synthesis. The pattern matches that of Vallina et al. (2015) for Nd-hydroxylbastnäsite ($NdCO_3OH$).

The autoclave solubility experiments were divided into two sets. The first set of experiments was conducted under acidic conditions. Five solutions of variable $pH_{25°C}$ (1.305, 1.613, 2.098, 2.540, 3.00) were prepared by slowly adding concentrated HCl (Fisher Scientific, TraceMetal Grade) to deionized water (DI). One molality (mol/kg) of NaCl was added to each solution to ensure there was a constant presence of NaCl to satisfy the activity model used in our calculations (see below). Before each experiment, small quartz tubes containing synthesized Nd-hydroxylbastnäsite, capped with a porous Teflon film, were introduced into Teflon-lined autoclaves and submerged in 10mL of the experimental solution that previously had been introduced into the autoclaves. Next, a small piece of $CO_{2(s)}$ (dry ice; 0.3-1.3 grams) was added to the solutions and the autoclaves were immediately sealed with a Teflon O-ring. The autoclaves were weighed before and after adding the dry ice to determine how much was added to each solution. Dry ice was required in these experiments because of the low solubility of CO_2 under acidic conditions; the experiments were conducted at elevated pressure to ensure CO_2 was dissolved in the solutions. The autoclaves were heated in a Muffle Furnace for 13 days. At the end

of the experiments, the autoclaves were removed from the furnace and quenched in a stream of cold air (the quench time was <25min). The autoclaves were weighed before and after the experiments to ensure there was no loss of CO_2. Next, the holders containing the Nd-hydroxylbastnäsite were removed and a 3mL aliquot of sulfuric acid was added to the solutions and left for 24 hours to dissolve any Nd that may have precipitated on the walls of the Teflon reactor during the quenching process. Finally, Nd concentrations were measured by Inductively Coupled Plasma Quadrupole Mass Spectrometry (ICP-QMS). A sketch of the experimental setup is shown in Figure 2a. Values of the parameters for the first set of experiments are reported in Table 1.

Table 1. Values of the experimental parameters for the acidic solubility experiments, including the temperature, the amount of $CO_{2(s)}$ added to each autoclave, the calculated pH_T and activity of $CO_{2(aq)}$, and the measured concentration of Nd. All experimental solutions contained 1m NaCl.

T (°C)	$CO_{2(s)}$ added (g)	log a $CO_{2(aq)}$	pH_T	log m Nd
175	0.5	-1.002	2.023	-3.362
175	0.3	-1.128	2.271	-3.539
175	0.6	-0.997	2.779	-3.909
175	0.5	-1.017	3.251	-4.775
175	0.6	-0.997	3.626	-4.881
200	0.6	-0.928	2.032	-3.594
200	1	-0.861	2.287	-3.883
200	0.7	-0.931	2.787	-4.033
200	0.6	-0.926	3.289	-4.309
200	0.3	-1.078	3.587	-4.860
225	0.5	-0.878	2.097	-3.298
225	0.9	-0.765	2.383	-3.587
225	1	-0.772	2.915	-4.036
225	0.5	-0.869	3.464	-4.606
225	0.4	-0.925	3.771	-5.191
250	0.8	-0.757	2.152	-3.278
250	0.5	-0.800	2.483	-3.613
250	0.9	-0.816	3.046	-4.488
250	0.8	-0.767	3.491	-4.781
250	1.3	-0.718	3.837	-5.259

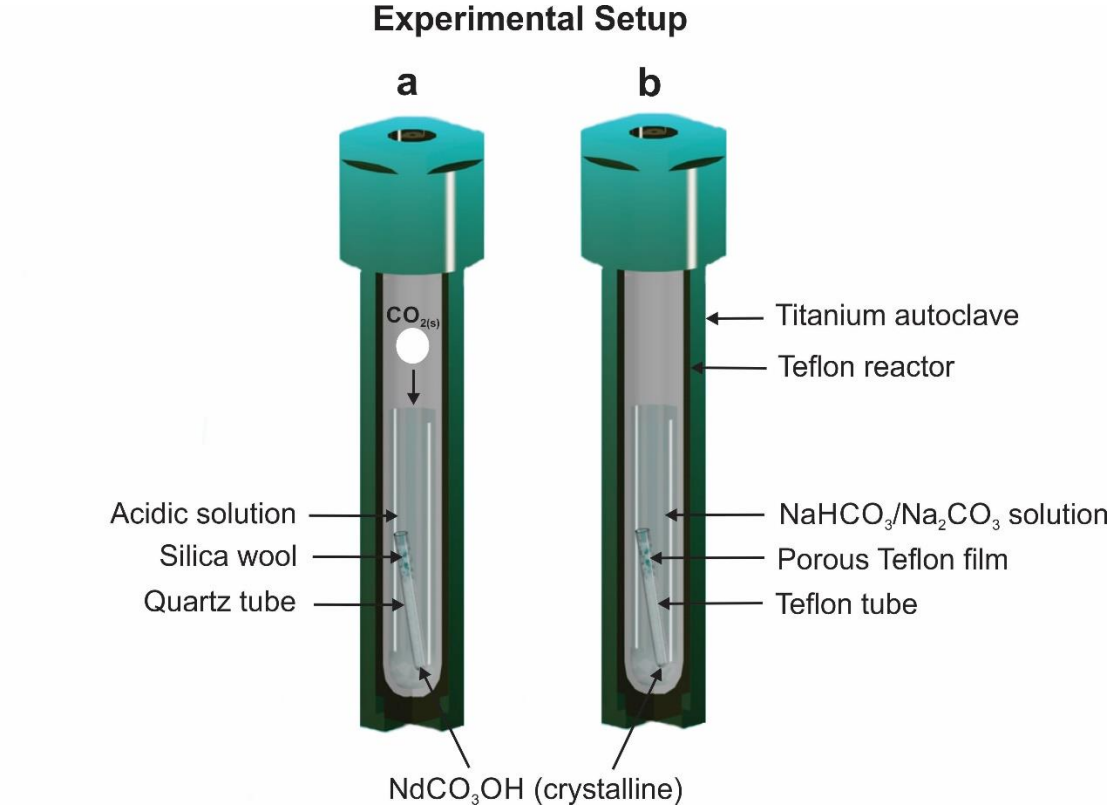

Figure 2a-b. A schematic cross-section depicting the experimental setup of the autoclave solubility method: a) Experiments conducted under acidic conditions using $CO_{2(s)}$ as the carbonate source and b) Experiments conducted at alkaline conditions using $NaHCO_3$ and Na_2CO_3 as the carbonate source.

The second set of solubility experiments was performed in alkaline solutions of varying carbonate concentration, and was conducted at the same temperatures as the experiments in acidic solutions. Two types of experimental solution were used to determine the solubility of Nd as a function of carbonate activity and pH: 1) solutions containing 0.05-0.5 m $NaHCO_3$; and 2) solutions containing 0.05-0.5 m Na_2CO_3, each containg 1 m NaCl. Targeted amounts of $NaHCO_3$ (Acros Organics, A.C.S. grade), Na_2CO_3 (anhydrous, Fisher Chemical, A.C.S. grade), and NaCl (Fisher Chemical, A.C.S. grade) were added to vacuum-degassed deionized water (DI) that was flushed with argon gas immediately before sealing the autoclaves to minimize the exchange of CO_2 between the fluid and the atmosphere. The experiments were heated for 7-21 days. The post-experimental steps were identical to those described above. A sketch of the experimental setup is

shown in Figure 2b. Valus of the parameters for the second set of experiments are reported in Table 2.

Table 2. Values of the experimental parameters for the alkaline solubility experiments, including the temperature, the amount of $NaHCO_3$ or Na_2CO_3 added to each autoclave, the calculated activity of HCO_3^- and pH_T, and the measured concentration of Nd. All experimental solutions contained 1m NaCl.

T (°C)	m $NaHCO_3$	m Na_2CO_3	log a HCO_3^-	pH_T	log m Nd
175	0.1		-1.380	7.855	-5.195
175	0.15		-1.208	7.857	-5.657
175	0.2		-1.087	7.856	-5.367
175	0.25		-0.993	7.853	-5.616
175	0.3		-0.917	7.85	-5.402
175	0.4		-0.799	7.842	-5.280
175		0.15	-1.792	9.594	-5.279
175		0.2	-1.730	9.653	-6.244
175		0.25	-1.685	9.696	-5.332
175		0.3	-1.649	9.73	-5.853
175		0.35	-1.620	9.757	-5.163
175		0.4	-1.595	9.78	-5.275
175		0.45	-1.574	9.799	-5.980
200	0.2		-1.148	7.962	-5.851
200	0.25		-1.055	7.96	-5.669
200	0.3		-0.980	7.958	-5.139
200	0.4		-0.863	7.951	-5.752
200	0.45		-0.816	7.947	-5.742
200		0.1	-1.851	9.412	-5.572
200		0.15	-1.757	9.505	-5.626
200		0.2	-1.695	9.566	-5.249
200		0.25	-1.649	9.61	-6.211
200		0.3	-1.614	9.645	-5.216
200		0.35	-1.585	9.673	-5.658
225	0.2		-1.221	8.086	-4.577
225	0.25		-1.129	8.086	-5.517
225	0.3		-1.055	8.084	-5.204
225	0.35		-0.993	8.082	-5.033
225	0.4		-0.940	8.079	-4.367
225	0.45		-0.893	8.075	-5.344
225		0.05	-2.031	9.175	-4.803
225		0.1	-1.847	9.357	-4.392
225		0.15	-1.750	9.453	-4.813
225		0.2	-1.687	9.516	-4.769
225		0.25	-1.641	9.562	-4.692

225		0.3	-1.605	9.597	-4.197
225		0.35	-1.576	9.626	-5.172
225		0.4	-1.552	9.65	-4.943
250	0.05		-1.895	8.15	-5.240
250	0.1		-1.598	8.204	-5.078
250	0.15		-1.428	8.222	-4.909
250	0.2		-1.309	8.229	-5.031
250	0.25		-1.218	8.231	-4.955
250	0.3		-1.144	8.23	-5.068
250	0.35		-1.083	8.229	-4.877
250	0.4		-1.031	8.226	-4.749
250	0.45		-0.985	8.223	-4.871
250		0.1	-1.871	9.341	-4.706
250		0.15	-1.772	9.44	-4.916
250		0.2	-1.707	9.505	-5.228
250		0.25	-1.660	9.552	-4.881
250		0.3	-1.625	9.588	-4.658
250		0.35	-1.596	9.617	-4.921
250		0.4	-1.572	9.641	-4.967
250		0.45	-1.553	9.661	-4.776

The time required to reach a steady-state Nd concentration in the experiments was determined through time-series experiments, in which autoclaves containing solutions of identical composition (e.g. 0.2m $NaHCO_3$ and 1m NaCl) were heated at 175°C and removed sequentially over 7 days. It was determined that a steady-state concentration was reached in less than 3 days for all experimental solutions (Fig. 3); the time would have been less at higher temperature because of a higher rate of reaction. All the experiments had a minimum duration of 7 days. To prevent contamination, the Teflon reactors and titanium autoclaves were soaked for more than 48 hours in a 5% nitric acid solution (Fisher Chemical, TraceMetal Grade), prepared with deionized water between experiments.

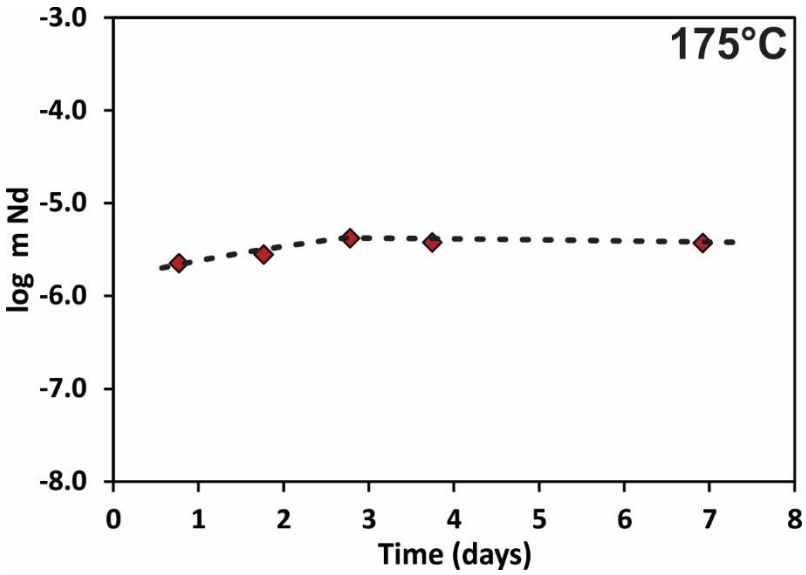

Figure 3. An example of the time series experiments. Each autoclave contained 0.2m $NaHCO_3$ and 1m NaCl. As shown in the figure, a steady-state concentration of Nd was achieved in less than 3 days.

4. Results and Data Treatment

The results of the first set of solubility experiments conducted under acidic conditions are reported in Table 1. This table lists the logarithm of the measured concentration of dissolved Nd, the amount of $CO_{2(s)}$ added to each autoclave, the calculated activity of $CO_{2(aq)}$ dissolved in the solution, and the pH of the solution calculated at the experimental temperature (pH_T). We used the thermodynamic modeling software, HCh, to calculate the activity of dissolved $CO_{2(aq)}$ and pH_T, (Shvarov and Bastrakov, 1999). The model that was employed included the following aqueous species: H_2O, H^+, OH^-, O_2, H_2, Na^+, NaOH°, NaCl°, Cl^-, HCl°, $NaCO_3^-$, $NaHCO_{3(aq)}$, CO_2, CO_3^{2-}, and HCO_3^- with thermodynamic data taken from Johnson et al. (1992), Shock et al. (1997), Sverjensky et al. (1997), Tagirov et al. (1997), and Miron et al. (2017). The thermodynamic properties of water and its dissociation constant were calculated using the Haar-Gallagher-Kell model (Kestin et al., 1984) and the Marshall and Franck model (Marshall and Franck, 1981), respectively. To date, the most reliable and accurate thermodynamic calculations for high temperature are those performed in NaCl-dominant solutions (Oelkers and Helgeson, 1991). This

limitation is due to the relative paucity of activity models tuned and experimentally verified at elevated temperature for other background electrolytes. The lack of an experimentally proven activity model is the reason why all the experiments were designed to be NaCl-dominant. The model used in these, and all subsequent calculations was the extended Debye-Hückel model modified by Helgeson et al. (1981), Oelkers and Helgeson (1990), and Oelkers and Helgeson (1991), which is recommended for NaCl-dominated solutions up to an ionic strength of 6, and a temperature up to 600°C:

$$\log \gamma_i = -\frac{AZ_i^2\sqrt{I}}{1+B\dot{a}\sqrt{I}} + b_\gamma I + \Gamma \quad (1)$$

where A and B are the Debye-Hückel solvent parameters, γ_i, Z_i and $\dot{a}_\iota$ are the individual molal activity coefficient, the charge, and the distance of the closest approach of an ion *i*, respectively. The effective ionic strength calculated using the molal scale is I, Γ is a molarity to molality conversion factor, and b_γ is the extended-term parameter for NaCl from Helgeson et al. (1981). The species $CO_{2(gas)}$ (Holland and Powell, 1998) was included in the model as a perfectly mobile component, and the fugacity of CO_2 in the experimental solutions was calculated using the modified Redlich–Rosenfeld equation of Appelo et al. (2014). The activity of dissolved $CO_{2(aq)}$ and pH_T were calculated iteratively and are reported in Table 1.

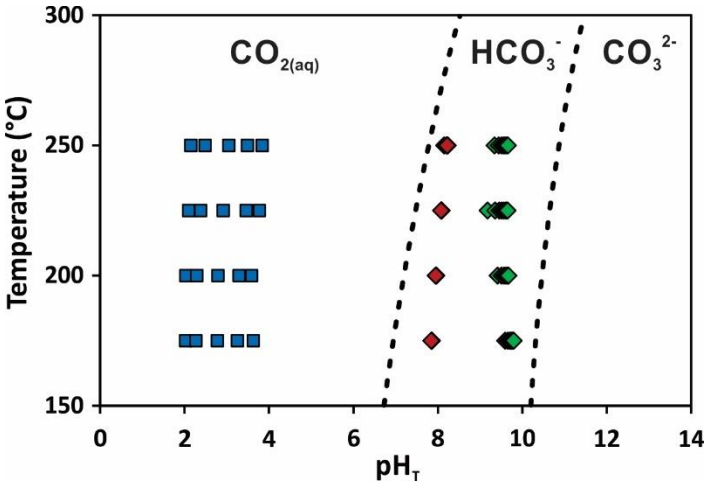

Figure 4. A predominance diagram for dissolved carbonate species as a function of pH_T and temperature. The experimental data points are plotted on the figure to show which carbonate species predominates at the experimental conditions. The blue squares correspond to the acidic experiments, the red diamonds to the experiments with $NaHCO_3$, and the green diamonds to the experiments with Na_2CO_3.

The results and values of the parameters for the solubility experiments conducted under alkaline conditions (pH_T 7.8 − 9.8) are reported in Table 2, and include the concentration of dissolved Nd measured in the experimental solutions, the amount of $NaHCO_3$ or Na_2CO_3 added to the solutions, the calculated pH_T, and the calculated activity of HCO_3^-. The activity of HCO_3^- was determined for each experiment using the model described above. Preliminary calculations demonstrate that less than 0.1% of CO_2 is partitioned into the gas phase at these conditions, so $CO_{2(gas)}$ was excluded from these calculations.

3.2 Determination of predominant Nd aqueous species in acidic, carbonate-bearing solutions

Multiple Nd aqueous species were considered when analyzing the experimental data collected under acidic conditions. These comprise Nd^{3+}, $NdCl^{2+}$, $NdCl_2^+$, $NdCO_3^+$, and $Nd(CO_3)_2$. Polynuclear species were not considered as it can be assumed that these species become unstable at high temperatures due to the decrease in the dielectric constant of water and the associated increase in electrostatic repulsion at elevated temperature (Brugger et al., 2014; Seward et al.,

2014). As shown in Figure 4, all experimental data points fall within the predominance field of $CO_{2(aq)}$. Thus, to determine the dominant aqueous complex, the logarithm of the concentration of Nd was plotted as a function of the pH_T and the logarithm of the activity of $CO_{2(aq)}$, normalized to a pH of 0 and activity of $CO_{2(aq)}$ of 1 in accordance with the stoichiometry of the considered reaction. For example, the reaction for the formation of $Nd(CO_3)_2^-$ is:

$$NdCO_3OH + CO_{2(aq)} \leftrightarrow Nd(CO_3)_2^- + H^+ \quad (2)$$

When plotted as a function of the logarithm of the activity of $CO_{2(aq)}$, the logarithm of the measured concentration of Nd, normalized to a pH_T of 0, should increase linearly with a slope of +1. In addition, when plotted as a function of increasing pH_T, the logarithm of the concentration of Nd, normalized to a $CO_{2(aq)}$ activity of 1 should increase with a slope of +1. The experimental data do not follow the predicted trends for the predominance of $Nd(CO_3)_2^-$ and thus this complex was deemed unlikely to be present in the experiments in significant quantities. Similar exercises were carried out for the other Nd complexes considered.

Our data indicate that the dominant aqueous complex at the experimental conditions is $NdCO_3^+$, formed by the reaction:

$$NdCO_3OH + H^+ \leftrightarrow NdCO_3^+ + H_2O \quad (3)$$

The expected trends for the predominance of $NdCO_3^+$ are: 1) If plotted as a function pH_T, the logarithm of the concentration of Nd should decrease with a slope of -1; and 2) if plotted as a function of the logarithm of the activity of $CO_{2(aq)}$, the logarithm of the concentration of Nd, normalized by adding pH_T, should have a slope of 0, owing to the absence of $CO_{2(aq)}$ in the above reaction. As shown in Figures 5 and 6, the observed trends are consistent with those predicted for $NdCO_3^+$. No detectable dependence on $CO_{2(aq)}$ was observed.

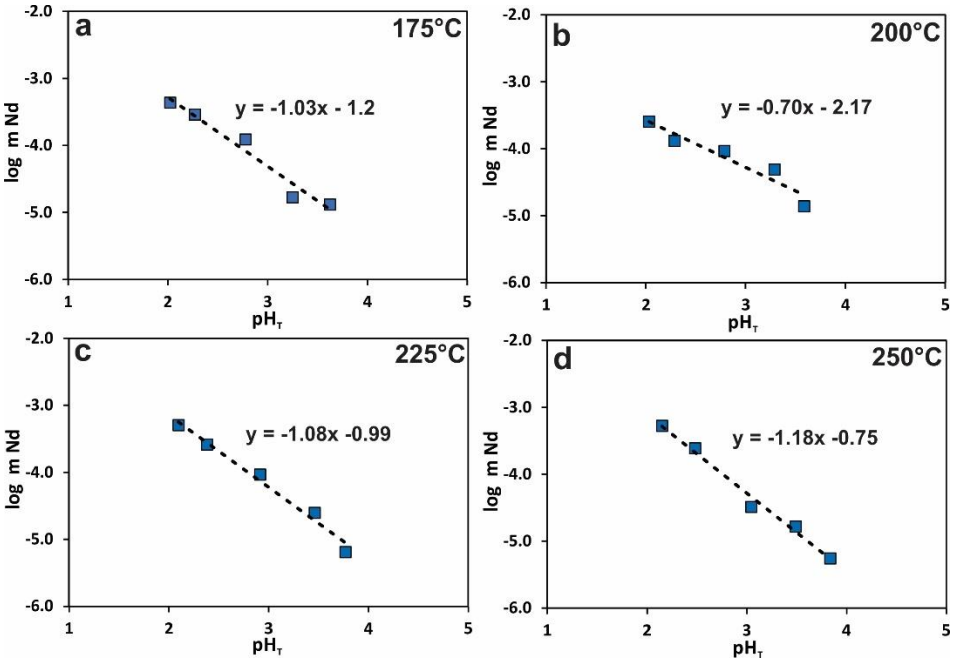

Figure 5. The concentrations of Nd for the experiments conducted under acidic solutions, plotted as a function of pH_T.

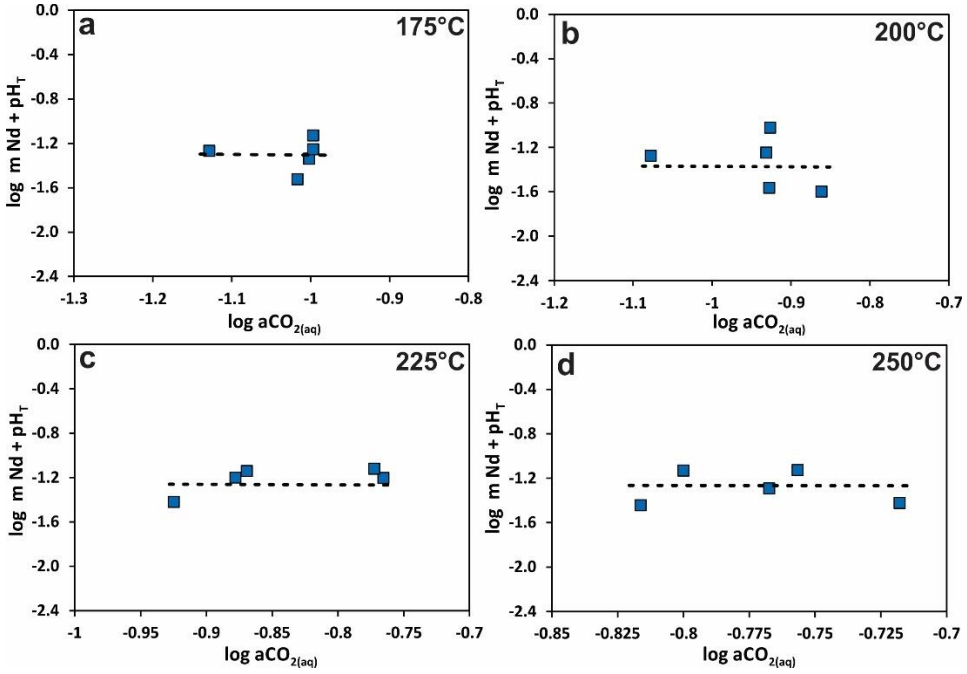

Figure 6. The concentrations of Nd for the experiments conducted under acidic solutions, plotted as a function of the logarithm of the activity of $CO_{2(aq)}$, normalized to the stoichiometry of $NdCO_3^+$.

3.2 Determination of predominant Nd aqueous species in alkaline, carbonate-bearing solutions

Irrespective of whether $NaHCO_3$ or Na_2CO_3 was added to the solutions, the conditions of the experiments corresponded to those of the predominance field of HCO_3^- (Fig. 4). Therefore, to evaluate whether Nd-carbonate species predominate in solution, the logarithm of the concentration of Nd was plotted as a function of the activity of HCO_3^- for both sets of experiments (Figs. 7 and 8). As shown in Figures 7 and 8, the concentration of Nd is independent of the activity of HCO_3^- over the entire temperature range, for all experiments. To analyze the pH dependency of the saturation concentration of Nd in our experimental solutions, the two sets of experimental data, each of which had a specific pH controlled by the molality of $NaHCO_3$ or Na_2CO_3 added to the starting solution, were plotted as a function of their calculated pH_T for each experimental temperature. As shown in Figure 9, the concentration of Nd was also independent of the pH_T at all temperatures investigated. Thus, our experimental results suggest that the predominant Nd aqueous complex at all temperatures investigated is $NdCO_3OH_{(aq)}$, formed via the congruent dissolution of the phase, Nd-hydroxylbastnäsite:

$$NdCO_3OH_{solid} \leftrightarrow NdCO_3OH_{aqueous} \quad (4)$$

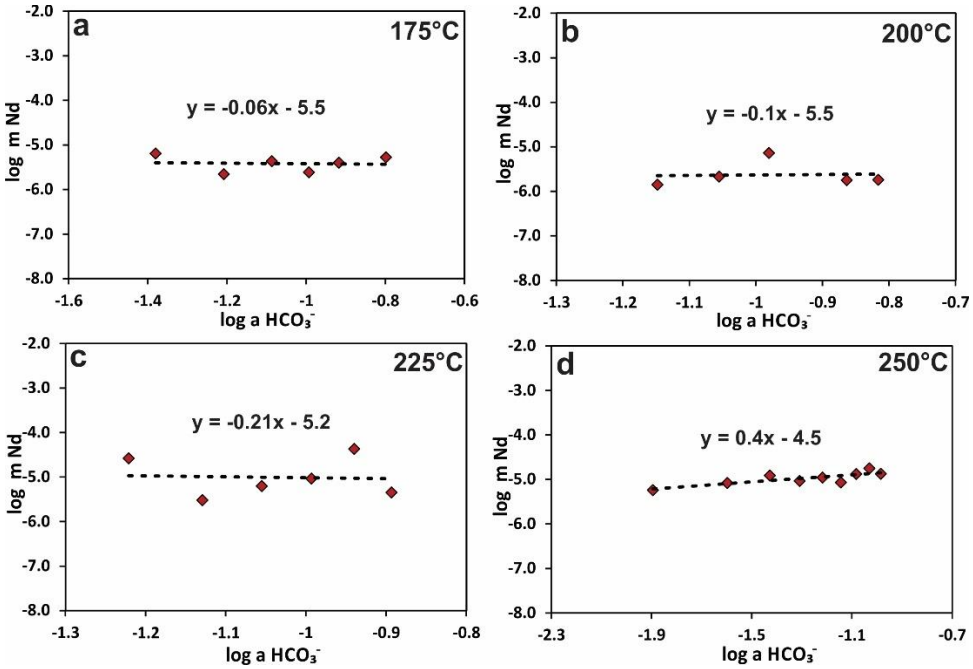

Figure 7a-d. The concentration of Nd determined from the $NaHCO_3$ experiments. The logarithm of the concentration of Nd is plotted as a function of the logarithm of the activity of HCO_3^- at a) 175°C, b) 200°C, c) 225°C, and d) 250°C. No dependence of Nd concentration on the activity of HCO_3^- was detected.

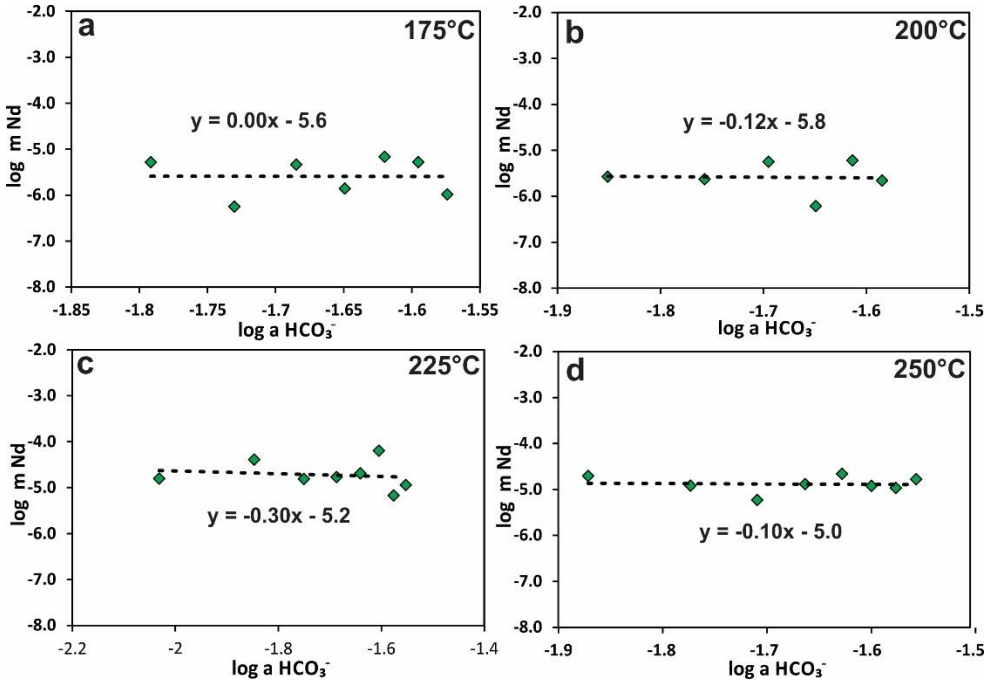

Figure 8a-d. The concentration of Nd determined from the Na_2CO_3 experiments. The logarithm of the concentration of Nd is plotted as a function of the logarithm of the activity of HCO_3^- at a) 175°C, b) 200°C, c) 225°C, and d) 250°C. No dependence of Nd concentration on the activity of HCO_3^- was detected.

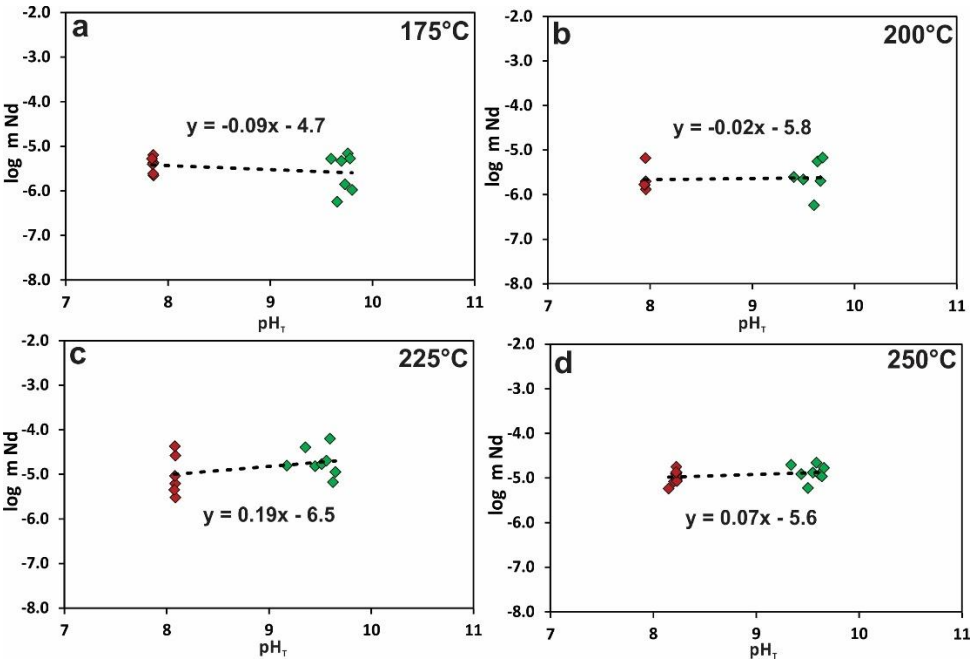

Figure 9a-d. The concentration of Nd obtained in the $NaHCO_3$ (red diamonds) and Na_2CO_3 (green diamonds) experiments plotted as a function of pH_T. No significant dependence of Nd concentration on pH_T was detected.

3.2 Derivation of thermodynamic data

The data collected in this study were used to calculate the solubility constants (*log K*) for $NdCO_3^+$ and $NdCO_3OH_{(aq)}$ at each experimental temperature via the following reactions:

$$NdCO_3OH_{(s)} + H^+ \leftrightarrow NdCO_3^+ + H_2O \quad (5)$$

$$log\ K = \log a\ NdCO_3^+ + \log a\ H_2O - \log a\ NdCO_3OH_{(s)} + pH \quad (6)$$

$$NdCO_3OH_{(s)} \leftrightarrow NdCO_3OH_{(aq)} \quad (7)$$

$$log\ K = \log a\ NdCO_3OH_{(aq)} - \log a\ NdCO_3OH_{(s)} \quad (8)$$

We were unable to measure the solubility of Nd-hydroxylbastnäsite at conditions corresponding to the predominance of non-carbonate Nd complexes. Because of this, and considering that a complete thermodynamic dataset for Nd-hydroxylbastnäsite does not exist, derivation of the thermodynamic formation constants (log β) was not possible. Therefore, we report only the

solubility constants (log *K*) for the formation of the Nd-carbonate complexes with respect to Nd-hydroxylbastnäsite (Table 3). Further studies focused on the thermodynamic characterization of hydroxylbastnäsite at elevated temperatures or Nd complexation in solutions containing detectable non-carbonate aqueous complexes (e.g., through UV-Vis spectroscopy) are required to determine the formation constants for $NdCO_3^+$ and $NdCO_3OH_{(aq)}$.

Table 3. Calculated log Ks for $NdCO_3^+$ (Reaction 6) and $NdCO_3OH_{(aq)}$ (Reaction 8) based on the experimental data.

T (°C)	log K	
	$NdCO_3^+$	$NdCO_3OH_{(aq)}$
175	-1.303	-5.511
200	-1.339	-5.608
225	-1.217	-4.845
250	-2.281	-4.931

5. Discussion

The experimental data collected in this study demonstrate that Nd forms stable complexes with CO_3^{2-} over a wide range of pH at temperatures relevant to hydrothermal fluids. As shown in Figure 10, $NdCO_3^+$ predominates in acidic solutions (pH_T 2 − 4), and promotes the significant dissolution of Nd-hydroxylbastnäsite, with concentrations of Nd reaching 58 ppm in the experimental solutions. For reference, the reconstructed concentration of Nd in fluid inclusions collected from the REE-bearing Capitan Pluton in New Mexico ranged from 19-190 ppm (Banks et al., 1994). However, it should be mentioned these values did not correspond to the dissolution of hydroxylbastnäsite. As pH increases, the concentration of Nd decreases by 1 logarithmic unit per unit of pH until it reaches a solubility minimum (~1 ppm Nd) at a pH_T of ~4. The concentration of Nd remains constant as pH is raised further owing to the formation and predominance of $NdCO_3OH_{(aq)}$, the dissolution reaction of which is independent of pH (Fig. 10).

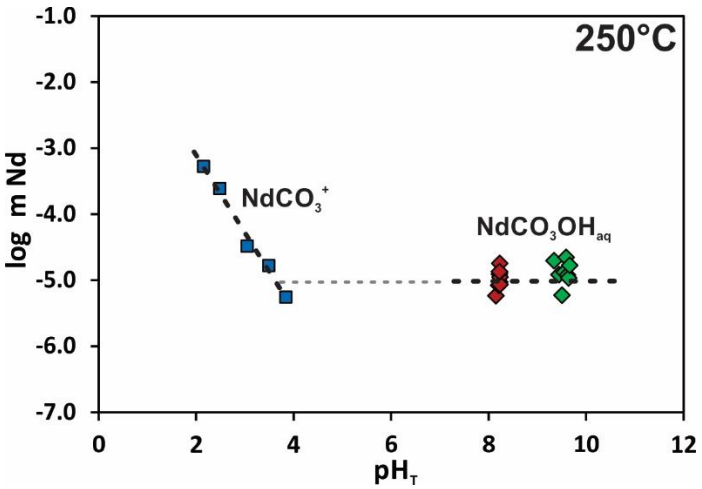

Figure 10. An example of the experimentally determined concentration of Nd plotted together as a function of pH_T for 250°C. The grey dashed line is the predicted trend.

Our experiments demonstrate that there is potential for significant dissolution of Nd in carbonate-bearing hydrothermal solutions. However, it is clear that our autoclave experiments are highly simplified, and are not entirely representative of natural hydrothermal systems. For example, REE minerals invariably occur as solid solutions in nature, which we did not account for in our experiments. Furthermore, hydroxylbastnäsite is uncommon in nature and bastnäsite most commonly found is close to its fluorobastnäsite endmember ($NdCO_3F$), which is more stable (Voigt et al., 2016). If we were to have considered the solubility of $NdCO_3F_{(s)}$ in our experiments and assumed that the same aqueous species predominated in solution, the predicted solubility of Nd as a function of pH would change substantially; the concentration of Nd would be independent of pH under acidic conditions for which $NdCO_3^+$ predominates, and increase by 1 logarithmic unit per unit of pH under alkaline conditions with the formation of $NdCO_3OH_{(aq)}$. Although this assessment is qualitative, it suggests that the concentration of dissolved Nd could be significant at elevated pH, and thus, the formation of Nd-hydroxyl-carbonate complexes could be an efficient mechanism for the transport of Nd under near-neutral and alkaline conditions. The identification of these complexes also removes the need for alkali-dominated (Na and K) REE complexes to

promote REE mobilization in hydrothermal systems, as has been proposed by Anenburg et al. (2020). Moreover, although previous studies have largely attributed REE mobilization at ore-grade concentrations to the formation of REE-chloride and sulfate complexes in acidic fluids (Migdisov et al., 2016), our findings suggest that alkaline solutions and the formation of REE-hydroxyl-carbonate complexes should also be considered as potentially important means of REE transport. Indeed, Nd-carbonate complexes predominated over Nd-chloride complexes in our experiments.

Although there have been few experimental studies of the speciation of the REE in alkaline solutions at elevated temperature, recent experimental results reported by Louvel et al. (2022), based on in-situ X-ray Absorption Spectroscopy (XAS), corroborate our findings by identifying hydroxyl-carbonate complexes in alkaline solutions at temperatures up to 500°C (these complexes are interpreted to be polynuclear species). These authors further demonstrated an apparent fractionation of the REE with temperature, in which hydroxyl-carbonate complexation led to the preferential mobilization of the LREE and HREE at $T > 300$°C and $T < 300$°C, respectively (Louvel et al., 2022). Together, these findings suggest that previous models on the genesis of REE ore deposits by acidic hydrothermal fluids should be re-assessed.

Carbonatite intrusions and their associated weathering and alteration products are major sources for economic REE extraction. Despite their prevalence, the mechanisms in which the REE are mobilized and enriched in these deposits have not yet been resolved. Determining the exact composition of a hydrothermal ore-forming fluid is challenging, which has led researchers to assume these fluids to be acidic, regardless of whether the pH of the solution is known (Beland and Williams-Jones, 2021). However, as highlighted by Louvel et al. (2022), the acidic transport and concentration of the REE often contradict field observations of carbonatite-hosted REE deposits, including the occurrence of abundant calcite veins associated with REE minerals (Jia and

Liu, 2019), and carbonate minerals formed by hydrothermal alteration (Beland and Williams-Jones, 2021). Recent direct measurements of the compositions of the compositions of fluid inclusions in the Strange Lake REE deposit in Canada, coupled with estimates of temperature and pH showed that the ore fluids evolved from being extremely alkaline (up to pH 10 at 425°C) to quite acidic (pH of 3 at 300 °C). Importantly from the perspective of this study, the early fluids transported relatively high concentrations of the REE, and were relative enriched in carbonate (Vasyukova and Williams-Jones, 2018). Although these authors were unable to make direct measurements of carbonate anions, they predicted through charge balance, the high proportion of aqueous-carbonic inclusions and presence of nahcolite, that HCO_3^- is an important ligand in the solutions with high pH. The authors proposed that the transport of the REE in these fluids could have been facilitated by the formation of hydroxyl-fluoride complexes, based on thermodynamic data collected at low T. However, given the experimental results of this study, hydroxyl-carbonate complexes may also have been important in REE mobilization in these fluids. Unfortunately, a comprehensive evaluation of this and other hydrothermal systems, as well as the relative stability of Nd-carbonate versus fluoride, chloride and sulfate complexes is not possible at this time, due to the lack of thermodynamic data for Nd-hydroxylbastnäsite. The addition of these data would permit the derivation of thermodynamic formation constants for the aqueous species identified in this study, which could be incorporated into thermodynamic models to assess the role of these complexes and alkaline solutions on the formation of hydrothermal REE deposits. As a path forward, we foresee future experimental studies focused on deriving the thermodynamic stability of bastnäsite ($NdCO_3(OH,F)$), as well as thermodynamic formation constants ($log\ \beta$) for Nd-carbonate complexes via spectroscopic techniques (e.g. UV-Vis and Raman).

6. Conclusions

The experimental data presented in this study demonstrate that Nd forms stable complexes with carbonate ions at elevated temperature (175-250°C). Our results indicate that in acidic solutions (pH < 4), the dominant aqueous complex is $NdCO_3^+$, whereas in neutral to alkaline solutions, the $NdCO_3OH_{(aq)}$ complex predominates. Solubility constants were derived for each species at the experimental temperatures with respect to Nd-hydroxylbastnäsite. A complete thermodynamic characterization of Nd-hydroxylbastnäsite is required for further analysis of the stability of these complexes. Our results suggest that Nd-carbonate complexes could lead to significant dissolution and, thus, transport of Nd in hydrothermal fluids. The potential for alkaline solutions to transport the REE, particularly for deposits associated with carbonatites, should therefore be re-assessed.

7. Acknowledgments

We thank Oana Marina and Chelsea Neil for their assistance with the ICP-MS analyses, and Marley Rock and Kirsten Sauer for their help with XRD analyses. Research presented in this article was supported by the Office of Science, U.S. Department of Energy, Grant No. DE-SC002226, and by Los Alamos National Laboratory's (LANL) Center for Space and Earth Sciences (CSES). CSES is funded by LANL's Laboratory Directed Research and Development (LDRD) program under project number 20180475DR.

8. References

Anenburg M., Mavrogenes J. A., Frigo C. and Wall F. (2020) Rare earth element mobility in and around carbonatites controlled by sodium, potassium, and silica. *Sci. Adv.* **6**.

Appelo C. A. J., Parkhurst D. L. and Post V. E. A. (2014) Equations for calculating hydrogeochemical reactions of minerals and gases such as CO2 at high pressures and temperatures. *Geochimica et Cosmochimica Acta* **125**, 49–67.

Banks D. A., Yardley B. W. D., Campbell A. R. and Jarvis K. E. (1994) REE composition of an aqueous magmatic fluid: A fluid inclusion study from the Capitan Pluton, New Mexico, U.S.A. *Chemical Geology* **113**, 259–272.

Beland C. M. J. and Williams-Jones A. E. (2021) The genesis of the Ashram REE deposit, Quebec: Insights from bulk-rock geochemistry, apatite-monazite-bastnäsite replacement reactions and mineral chemistry. *Chemical Geology* **578**, 120298.

Brugger J., Tooth B., Etschmann B., Liu W., Testemale D., Hazemann J.-L. and Grundler P. V. (2014) Structure and Thermal Stability of Bi(III) Oxy-Clusters in Aqueous Solutions. *Journal of Solution Chemistry* **43**, 314–325.

Cantrell K. J. and Byrne R. H. (1986) Rare earth element complexation by carbonate and oxalate ions. *Geochimica et Cosmochimica Acta* **51**, 597–605.

Castor S. B. (2008) The Mountain Pass rare-earth carbonatite and associated ultrapotassic rocks, California. *The Canadian Mineralogist* **46**, 779–806.

Gysi A. P. and Williams-Jones A. E. (2015) The thermodynamic properties of bastnäsite-(Ce) and parisite-(Ce). *Chemical Geology* **392**, 87–101.

Haas J. R., Shock E. L. and Sassani D. C. (1995) Rare earth elements in hydrothermal systems: Estimates of standard partial molal thermodynamic properties of aqueous complexes of the rare earth elements at high pressures and temperatures. *Geochimica et Cosmochimica Acta* **59**, 4329–4350.

Helgeson H. C., Kirkham D. H. and Flowers G. C. (1981) Theoretical prediction of the thermodynamic behavior of aqueous electrolytes at high pressures and temperatures: IV. Calculation of activity coefficients, osmotic coefficients, and apparent molal and standard and relative partial molal properties to 600°C. *American Journal of Science* **281**, 1249–1516.

Holland T. J. B. and Powell R. (1998) An internally consistent thermodynamic data set for phases of petrological interest. *Journal of Metamorphic Geology* **16**, 309–343.

Jia Y. and Liu Y. (2019) REE Enrichment during Magmatic–Hydrothermal Processes in Carbonatite-Related REE Deposits: A Case Study of the Weishan REE Deposit, China. *Minerals* **10**, 25.

Johannesson K. H. and Stetzenbach K. J. (1995) Speciation of the rare earth element neodymium in groundwaters of the Nevada Test Site and Yucca Mountain and implications for actinide solubility. *Applied Geochemistry* **10**, 565–572.

Johnson J. W., Oelkers E. H. and Helgeson H. C. (1992) SUPCRT92: a software package for calculating the standard molal thermodynamic properties of minerals, gases, aqueous species, and reactions from 1 to 5000 bar and 0 to 1000 °C. *Computational Geosciences* **18**, 899–947.

Kalintsev A., Migdisov A., Alcorn C., Baker J., Brugger J., Mayanovic R. A., Akram N., Guo X., Xu H., Boukhalfa H., Caporuscio F. A., Viswanathan H., Jove-Colon C., Wang Y., Matteo E. and Roback R. (2021) Uranium carbonate complexes demonstrate drastic decrease in stability at elevated temperatures. *Commun Chem* **4**, 120.

Kestin J., Sengers J. V., Kamgar-Parsi B. and Levelt Sengers J. M. H. (1984) Thermophysical properties of fluid H2O. *Journal of Physical and Chemical Reference Data* **13**, 601–609.

Louvel M., Etschmann B., Guan Q., Testemale D. and Brugger J. (2022) Carbonate complexation enhances hydrothermal transport of rare earth elements in alkaline fluids. *Nat Commun* **13**, 1456.

Luo Y.-R. and Byrne R. H. (2004) Carbonate complexation of yttrium and the rare earth elements in natural waters. *Geochimica et Cosmochimica Acta* **68**, 691–699.

Marshall W. L. and Franck E. U. (1981) Ion product of water substance, 0-1000 °C, 1-10,000 bars new International Formulation and its background. *Journal of Physical and Chemical Reference Data* **10**, 295–304.

Migdisov A. A. and Williams-Jones A. E. (2002) A spectrophotometric study of neodymium(III) complexation in chloride solutions. *Geochimica et Cosmochimica Acta* **66**, 4311–4323.

Migdisov A., Williams-Jones A. E., Brugger J. and Caporuscio F. A. (2016) Hydrothermal transport, deposition, and fractionation of the REE: experimental data and thermodynamic calculations. *Chemical Geology* **439**, 13–42.

Migdisov Art. A., Reukov V. V. and Williams-Jones A. E. (2006) A spectrophotometric study of neodymium(III) complexation in sulfate solutions at elevated temperatures. *Geochimica et Cosmochimica Acta* **70**, 983–992.

Migdissov A. A. and Williams-Jones A. E. (2007) An experimental study of the solubility and speciation of neodymium (III) fluoride in F-bearing aqueous solutions. *Geochimica et Cosmochimica Acta* **71**, 3056–3069.

Miron G. D., Wagner T., Kulik D. A. and Lothenbach B. (2017) An internally consistent thermodynamic dataset for aqueous species in the system Ca-Mg-Na-K-Al-Si-O-H-C-Cl to 800 °C and 5 kbar. *Am J Sci* **317**, 755–806.

Nisbet H., Migdisov A. A., Williams-Jones A. E., van Hinsberg V. J., Xu H. and Roback R. (2021) The solubility of thorium in carbonate-bearing solutions at hydrothermal conditions. *Geochimica et Cosmochimica Acta*, S001670372100260X.

Oelkers E. H. and Helgeson H. C. (1991) Calculation of activity coefficients and degrees of formation of neutral ion pairs in supercritical electrolyte solutions. *Geochimica et Cosmochimica Acta* **55**, 1235–1251.

Oelkers E. H. and Helgeson H. C. (1990) Triple-ion anions and polynuclear complexing in supercritical electrolyte solutions. *Geochimica et Cosmochimica Acta* **54**, 727–738.

Seward T. M., Williams-Jones A. E. and Migdisov A. A. (2014) The Chemistry of Metal Transport and Deposition by Ore-Forming Hydrothermal Fluids. In *Treatise on Geochemistry* Elsevier. pp. 29–57.

Shivaramaiah R., Anderko A., Riman R. E. and Navrotsky A. (2016) Thermodynamics of bastnaesite: A major rare earth ore mineral. *American Mineralogist* **101**, 1129–1134.

Shock E. L., Sassani D. C., Willis M. and Sverjensky D. A. (1997) Inorganic species in geological fluids: Correlations among standard molal thermodynamic properties of aqueous ions and hydroxide complexes. *Geochimica et Cosmochimica Acta* **61**, 907–950.

Shvarov Y. V. and Bastrakov E. (1999) HCh, A Software Package for Geochemical Equilibrium Modeling: User's Guide.

Sverjensky D. A., Shock E. L. and Helgeson H. C. (1997) Prediction of the thermodynamic properties of aqueous metal complexes to 1000 °C and 5 kb. *Geochimica et Cosmochimica Acta* **61**, 1359–1412.

Tagirov B. R., Zotov A. and Akinfiev N. (1997) Experimental study of dissociation of HCl from 350 to 500 °C and from 500 to 2500 bars: thermodynamic properties of HCl°(aq). *Geochimica et Cosmochimica Acta* **61**, 4267–4280.

Vallina B., Rodriguez-Blanco J. D., Blanco J. A. and Benning L. G. (2014) The effect of heating on the morphology of crystalline neodymium hydroxycarbonate, NdCO3OH. *Mineralogical Magazine* **78**, 1391–1397.

Vallina B., Rodriguez-Blanco J. D., Brown A. P., Blanco J. A. and Benning L. G. (2015) The role of amorphous precursors in the crystallization of La and Nd carbonates. *Nanoscale* **7**, 12166–12179.

Van Gosen B. S., Verplanck P. L., Seal II R. R., Long K. R. and Gambogi J. (2017) *Critical Mineral Resources of the United States—Economic and Environmental Geology and Prospects for Future Supply*.,

Vasyukova O. V. and Williams-Jones A. E. (2018) Direct measurement of metal concentrations in fluid inclusions, a tale of hydrothermal alteration and REE ore formation from Strange Lake, Canada. *Chemical Geology* **483**, 385–396.

Verplanck P. L. and Hitzman M. W. (2016) *Rare earth and critical elements in ore deposits*.,

Voigt M., Rodriguez-Blanco J. D., Vallina B., Benning L. G. and Oelkers E. H. (2016) An experimental study of hydroxylbastnasite solubility in aqueous solutions at 25 °C. *Chemical Geology* **430**, 70–77.

Voncken J. H. L. (2016) The Ore Minerals and Major Ore Deposits of the Rare Earths. In *The Rare Earth Elements* Springer International Publishing, Cham. pp. 15–52.

Voncken J.H.L. (2016) *The Rare Earth Elements*., Springer Berlin Heidelberg, New York, NY.

Wood S. A. (1990) The aqueous geochemistry of the rare-earth elements and yttrium 2. Theoretical predictions of speciation in hydrothermal solutions to 350°C at saturation water vapor pressure. *Chemical Geology* **88**, 99–125.